Energy Spectra in Rayleigh-Benard Convection

2011 J. Phys.: Conf. Ser. 318 082014

(http://iopscience.iop.org/1742-6596/318/8/082014)

Energy Spectra in Rayleigh-Bénard Convection

Mahendra K. Verma[1,⋆], Pankaj Mishra[1], Mani Chandra[1], and Supriyo Paul[2]

[1] Department of Physics, Indian Institute of Technology, Kanpur, India 208016
[2] Computational Fluid Dynamics Team, Scientific and Engineering Computation Group, Centre for Development of Advanced Computing, Pune, India 411007

E-mail: ⋆mkv@iitk.ac.in

Abstract. We present a numerical study of the energy spectra and fluxes in the inertial range of turbulent Rayleigh-Bénard convection for a wide range of Prandtl number. We consider both free-slip and no-slip conditions for our simulation. Our results support the Kolmogorov-Obukhov (KO) scaling for velocity field for zero-Prandtl number and low-Prandtl number ($P \ll 1$) convection. For large Prandtl number ($P > 1$) convection, the Bolgiano-Obukhov scaling (BO) appears to agree with the numerical results better than the KO scaling. We provide phenomenological arguments for the zero-Prandtl and low-Prandtl number convection.

1. Introduction

Turbulent thermal convection is ubiquitous in natural and engineering flows. Rayleigh-Bénard convection (RBC), in which a fluid confined between the plates is heated from below and cooled from the top, is an ideal model to study these phenomena. Two control parameters which govern the dynamics of RBC are: the Rayleigh number R, which is the ratio of buoyancy force to the stabilizing force, and the Prandtl number P, which is the ratio of the viscous diffusion coefficient to the thermal diffusion coefficient. One of the interesting problems of the turbulent convection is the scaling of the energy spectra and fluxes for its inertial range. In this paper we present numerical results of the energy spectra and fluxes in the inertial range of turbulent RBC for both free-slip and no-slip boundary conditions.

The presence of a buoyancy term makes the energy transfers in the inertial range of convective turbulence quite interesting and complex (Siggia (1994) and Lohse & Xia (2010)). For turbulent RBC, Procaccia & Zeitak (1989), L'vov (1991), and L'vov & Falkovich (1992) predicted that the kinetic energy spectrum scales as $E^u(k) \sim k^{-11/5}$ and the temperature (entropy) spectrum as $E^\theta(k) \sim k^{-7/5}$ [Bolgiano-Obukhov (BO) scaling] for scales above the Bolgiano length ($l_B < l < L$) in which buoyancy is the dominant force. For $l_d < l < l_B$, the inertia term dominates over the buoyancy force, and the kinetic energy and entropy spectra follow the Kolmogorov-Obukhov (KO) scaling, i.e., $E^u(k) \sim k^{-5/3}$, and $E^\theta(k) \sim k^{-5/3}$. Here, k is the wavenumber, L is the characteristic length scale, l_B is the buoyancy length scale, and l_d is the Kolmogorov length scale. In the BO regime, the entropy flux (Π^θ) is constant, while the kinetic energy flux (Π^u) varies as $k^{-4/5}$. However, in the KO regime, both the entropy and kinetic energy fluxes remain constant.

The energy transfers in the inertial range of turbulent RBC depends critically on the Prandtl number. It has been shown that for $P \ll 1$ (low-P fluid), l_B is of the order of the characteristic

scale L of the system, and hence, the KO scaling is expected to hold for low-P convection (Lohse & Xia (2010),Grossmann & L'vov (1993), Chilla *et al.* (1993), and Cioni *et al.* (1997)). However, for $P \gg 1$ (large-P fluid), l_B is smaller than the characteristic length scale, which gives rise to the coexistence of both the KO scaling and the BO scaling in the inertial range (Procaccia & Zeitak (1989), Grossmann & L'vov (1993), Chilla *et al.* (1993), Cioni *et al.* (1997)). A series of experiments (Chilla *et al.* (1993), Mashiko *et al.* (2004), Sun *et al.* (2006), Zhou & Xia (2001), Shang & Xia (2001), Castaing (1990), Ashkenazi & Steinberg (1999), Niemela *et al.* (2000), Cioni *et al.* (1995)) and numerical simulations (Borue & Orszag (1997), Skandera *et al.* (2009), Grossmann & Lohse (1991), Grossmann & Lohse (1992), Kerr (1996)) have been performed to test the above phenomenologies. Experiments by (Chilla *et al.* (1993), Wu *et al.* (1990), and Ashkenazi & Steinberg (1999)) performed in the range of $P \geqslant 0.7$ appear to support BO scaling, while experiments by Chilla *et al.* (1993) and Cioni *et al.* (1995) performed in the range of $P \leqslant 0.7$ tend to support KO scaling. Note, however, that Mashiko *et al.* (2004) reported only the presence of BO scaling for mercury ($P = 0.02$). Niemela *et al.* (2000) reported the coexistence of both BO and KO scaling for the temperature spectra of gaseous helium ($P \sim 0.7$) contained in a cylindrical container of aspect ratio one.

In this paper we numerically compute the energy and its cascade rate for a wide range of Prandtl numbers: Zero-P ($P = 0$), low-P ($P = 0.02$) and large-P ($P = 1, 6.8$). We compare the results with the existing phenomenologies and experimental observations.

2. Numerical Methods

The equations for the Rayleigh-Bénard convection under Boussinesq approximations are

$$\partial_t \mathbf{u} + (\mathbf{u}\cdot\nabla)\mathbf{u} = -\frac{\nabla\sigma}{\rho_0} + \alpha g\theta\hat{z} + \nu\nabla^2\mathbf{u}, \tag{1}$$

$$\partial_t \theta + (\mathbf{u}\cdot\nabla)\theta = \frac{\Delta}{d}u_z + \kappa\nabla^2\theta, \tag{2}$$

$$\nabla\cdot\mathbf{u} = 0 \tag{3}$$

where θ and σ are the temperature and pressure fluctuations from the steady conduction state ($T = T_c + \theta$, with T_c as the conduction temperature profile), $\hat{z}$ is the buoyancy direction, Δ is the temperature difference between the two plates, ρ_0 is the mean density of fluid, ν is the kinematic viscosity, and κ is the thermal diffusivity. For numerical simulations it is important to solve the nondimensionalized equations in order to reduce the number of parameters, as well as to keep the values of the variables to order one. The two important nondimensional parameters for the RBC are the Rayleigh number $R = \alpha g\Delta d^3/\nu\kappa$, and the Prandtl number $P = \nu/\kappa$. For the large Prandtl number, the nondimensional equations are

$$\frac{\partial\mathbf{u}}{\partial t} + (\mathbf{u}\cdot\nabla)\mathbf{u} = -\nabla\sigma + RP\theta\hat{z} + P\nabla^2\mathbf{u}, \tag{4}$$

$$\frac{\partial\theta}{\partial t} + (\mathbf{u}\cdot\nabla)\theta = u_3 + \nabla^2\theta, \tag{5}$$

when we use d as the length scale, κ/d as the velocity scale, and Δ as the temperature scale. Instead, when we use $\sqrt{\alpha\Delta g d}$ as the velocity scale, the equations become

$$\frac{\partial\mathbf{u}}{\partial t} + (\mathbf{u}\cdot\nabla)\mathbf{u} = -\nabla\sigma + \theta\hat{z} + \sqrt{\frac{P}{R}}\nabla^2\mathbf{u}, \tag{6}$$

$$\frac{\partial\theta}{\partial t} + (\mathbf{u}\cdot\nabla)\theta = u_3 + \frac{1}{\sqrt{PR}}\nabla^2\theta, \tag{7}$$

For the small Prandtl number fluids, we take the velocity scale as ν/d, and the temperature scale as $\nu\Delta/\kappa$, which yields the following nondimensional equations:

$$\frac{\partial \mathbf{u}}{\partial t} + (\mathbf{u}\cdot\nabla)\mathbf{u} = -\nabla\sigma + R\theta\hat{z} + \nabla^2\mathbf{u}, \quad (8)$$

$$P\left(\frac{\partial \theta}{\partial t} + (\mathbf{u}\cdot\nabla)\theta\right) = u_3 + \nabla^2\theta. \quad (9)$$

Note that for $P = 0$, Eq. (9) reduce to $u_3 + \nabla^2\theta = 0$. We could also nondimensionalize the above equations by choosing the velocity scale as $\sqrt{\alpha\Delta g d}$, which yields

$$\frac{\partial \mathbf{u}}{\partial t} + (\mathbf{u}\cdot\nabla)\mathbf{u} = -\nabla\sigma + P\theta\hat{z} + \sqrt{\frac{P}{R}}\nabla^2\mathbf{u}, \quad (10)$$

$$P\left(\frac{\partial \theta}{\partial t} + (\mathbf{u}\cdot\nabla)\theta\right) = u_3 + \sqrt{\frac{P}{R}}\nabla^2\theta, \quad (11)$$

The presence of boundary layers severely affects the dynamics in RBC (see e.g., Grossmann & Lohse (2000), Lohse & Xia (2010)). We choose two kinds of boundary conditions for the velocity fields at the horizontal plates: *free-slip* ($u_3 = \partial_z u_1 = \partial_z u_2 = 0$ at $z = 0, 1$) and *no-slip* ($u_1 = u_2 = u_3 = 0$ at $z = 0, 1$). For the temperature fields, we apply isothermal condition at the horizontal plates ($\theta = 0$ at $z = 0, 1$). For the free-slip case, periodic boundary condition is applied in the horizontal direction.

The nondimensional equations (Eqs. (1-3)) are solved for the free-slip boundary conditions using Pseudo-spectral code TARANG. For the details, refer to Mishra & Verma (2010) and the website http://turbulence.phy.iitk.ac.in. In brief, we consider a box of aspect ratio $2\sqrt{2} : 2\sqrt{2} : 1$ for the simulation. The time advancement is performed using fourth order Runge-Kutta (RK4) method. The detailed numerical and phenomenological studies of energy spectra and fluxes in a box with the free-slip boundary conditions are presented in Mishra & Verma (2010) for a wide range of Prandtl numbers: Zero-Prandtl number ($P = 0$), low-Prandtl number ($P = 0.02$), intermediate Prandtl number ($P = 0.2$) and large-Prandtl number ($P = 1, 6.8$). Note that, according to Kraichnan (1962), $P \geq 0.1$ is considered as large-Prandtl number. Here we briefly discuss some of the results reported by Mishra & Verma (2010).

The simulation for the no-slip boundary conditions on all the walls is performed using NEK5000, an open source spectral element code (Fischer (1997)). The simulation is performed in a two-dimensional (2D) box of aspect ratio $1 : 1$. For the temperature field, isothermal boundary condition is applied at the horizontal plates and adiabatic boundary condition at the vertical plates. We use 28×28 spectral elements and 15^{th} order polynomials for resolution inside the elements. Thus the effective grid resolution for the simulation is 420×420. Note that the grid is denser near the boundaries to resolve the boundary layer. After the simulation the velocity and temperature fields are interpolated to a regular grid of 384×384 resolution and a Fourier transformation is applied on them. For Fourier transformation we use PyFFTW3 (https://launchpad.net/pyfftw/), a Python wrapper for FFTW3 (http://www.fftw.org/). The three-dimensional simulations are underway, and they would be presented later. Relationship between the energy spectra of 2D and 3D RBC is still not clear , and it needs to be investigated further.

We compute the one-dimensional energy spectra of the velocity and temperature fields ($E^u(k)$ and $E^\theta(k)$ respectively) by summing up the energy of the Fourier modes in the shell $[k, k+1)$. The energy fluxes are defined using the "mode-to-mode energy transfers" formalism discussed in Verma (2004). According to this formalism, the kinetic energy flux Π^u and the entropy flux

Π^θ are

$$\Pi^u(k_0) = \sum_{k\geq k_0}\sum_{p<k_0}\delta_{\mathbf{k},\mathbf{p}+\mathbf{q}}\Im([\mathbf{k}\cdot\mathbf{u}(\mathbf{q})][\mathbf{u}^*(\mathbf{k})\cdot\mathbf{u}(\mathbf{p})]) \quad (12)$$

$$\Pi^\theta(k_0) = \sum_{k\geq k_0}\sum_{p<k_0}\delta_{\mathbf{k},\mathbf{p}+\mathbf{q}}\Im([\mathbf{k}\cdot\mathbf{u}(\mathbf{q})][\theta^*(\mathbf{k})\cdot\theta(\mathbf{p})]) \quad (13)$$

where $\Im$ represents the imaginary part of the argument. A word of caution is in order. The energy spectra and fluxes for the turbulent RBC is anisotropic. Yet, for simplicity, we report only the isotropic energy spectra and fluxes in the present paper. In the following section we will discuss the scaling of energy spectra and fluxes for different Prandtl numbers.

3. Results and Discussions

3.1. Zero-Prandtl number convection

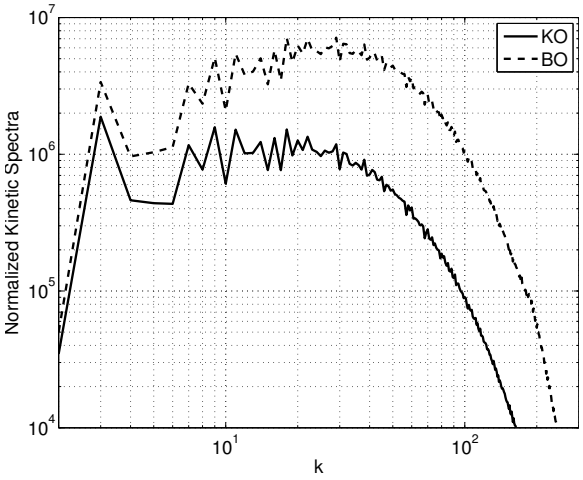

Figure 1. Compensated kinetic energy spectra $E^u(k)k^{5/3}$ (KO) and $E^u(k)k^{11/5}$ (BO) for $P = 0$ and $R = 1.97 \times 10^4$. This figure is taken from Mishra & Verma (2010).

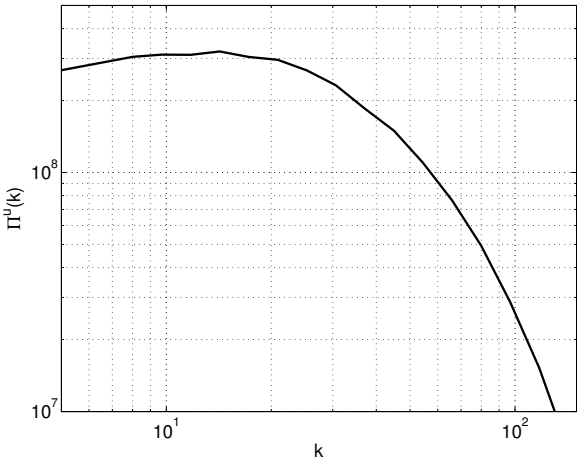

Figure 2. Kinetic flux for $P = 0$ convection. The constancy of flux in the inertial range indicates KO scaling. This figure is taken from Mishra & Verma (2010).

According to Eqs.(8-9), the temperature field is slaved to the vertical velocity for the zero-Prandtl number convection (the relationship being $\theta = -1/\nabla^2 u_3$). Therefore, the entropy spectra $E^\theta(k) \sim E^u/k^4$, which indicates that the buoyancy force is active at very small wavenumber only. Therefore Kolmogorov's theory of fluid turbulence must be valid here. Hence, the KO scaling should work for $P = 0$ convection.

We perform the direct numerical simulation for $P = 0$ at $R = 1.97 \times 10^4$ on a 256^3 grid and calculate the energy spectra and fluxes from the steady-state data. We solve the nondimensional equation (8) and $\theta(\mathbf{k}) = u_3(\mathbf{k})/k^2$ simultaneously. Fig. 1 exhibits the plots of compensated kinetic energy spectra $E(k)k^{5/3}$ and $E(k)k^{11/5}$ vs. k for this run. For the inertial range ($8 < k < 32$), the numerical results are in better agreement with Kolmogorov's 5/3 spectrum than BO's 11/5 spectrum, which is consistent with the phenomenological arguments presented above. The constancy of the kinetic energy flux (See Fig. 2) in the inertial range also support the KO scaling for $P = 0$.

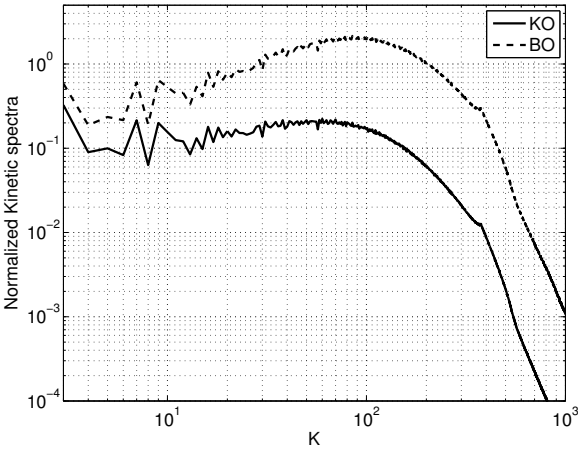

Figure 3. Compensated kinetic energy spectra $E^u(k)k^{5/3}$ (KO) and $E^u(k)k^{11/5}$ (BO) for $P = 0.02$ and $R = 2.6\times10^6$ on a 512^3 grid. The compensated spectrum fits better with the KO scaling than the BO scaling. This figure is taken from Mishra & Verma (2010).

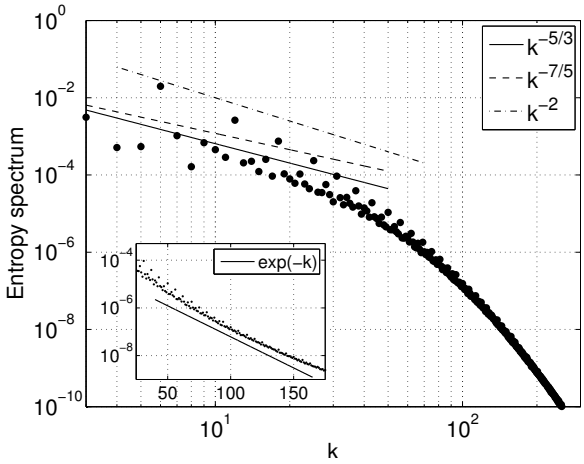

Figure 4. Entropy spectra for $P = 0.02$ and $R = 2.6 \times 10^6$ on a 512^3 grid. Inset shows the exponential nature of the entropy spectum. This figure is taken from Mishra & Verma (2010).

3.2. Low-Prandtl number convection

In the previous section we showed that the scaling of kinetic energy follows the KO scaling for $P = 0$ because buoyancy acts on a narrow low-wavenumber range. This phenomenological argument for validation of KO scaling for $P = 0$ can be extended to low-Prandtl number convection. For low-P convection, the estimated "Kolmogorov diffusion wavenumber" $k_c = (\Pi^u/\kappa^3)^{1/4}$ is much smaller compared to the "Kolmogorov dissipation wavenumber" $k_d = (\Pi^u/\nu^3)^{1/4}$ (Lesieur (2006)). Therefore we expect the phenomenology of the passive scalar (KO scaling) to work for $1 \ll k \ll k_c$. For $k_c \ll k \ll k_d$, the velocity field would continue to follow KO scaling, while the temperature field would be diffusive with an exponential spectrum $E(k) \sim \exp(-ck)$, where c is a constant (Lesieur (2006)).

We simulate the RBC equations (10-11) for $P = 0.02$ and compute the energy spectra and fluxes under the steady state. Fig. 3 exhibits the compensated kinetic energy spectra for this case. The numerical data in the inertial range fits better with the KO scaling than the BO scaling, consistent with the phenomenological arguments presented above.

We plot the entropy spectra in Fig. 4. We observe dual branches in the entropy spectra (Vincent & Yuen (1999) for 2D RBC and by Mishra & Verma (2010) for 3D RBC). Mishra & Verma (2010) show that the upper branch corresponds to the modes $\theta(0, 0, 2n)$ with $\theta(0, 0, 2n) \approx -1/(2n\pi)$, thus $E(k) \sim k^{-2}$. We expect the lower branch to correspond to the KO or BO scaling. However, since $k_c \sim 1$, the 5/3 power law region corresponding to the passive scalar is absent in the spectrum. The lower branch essentially exhibits a exponential (or dissipative) behaviour for $k_c < k < k_d$ (see Fig. 4 and its inset). The kinetic energy flux remains constant for a reasonably wide range of wavenumbers, while the entropy flux falls quite sharply in the inertial range (see Fig. 5). This behaviour of fluxes for $P = 0.02$ is consistent with the spectrum results and the phenomenological arguments presented above.

3.3. large-Prandtl number convection

We performed 3D RBC simulations for $P = 6.8$, a representative large Prandtl number. We solve Eqs. (6-7) under free-slip boundary conditions and compute the energy spectra and fluxes. Fig. 6

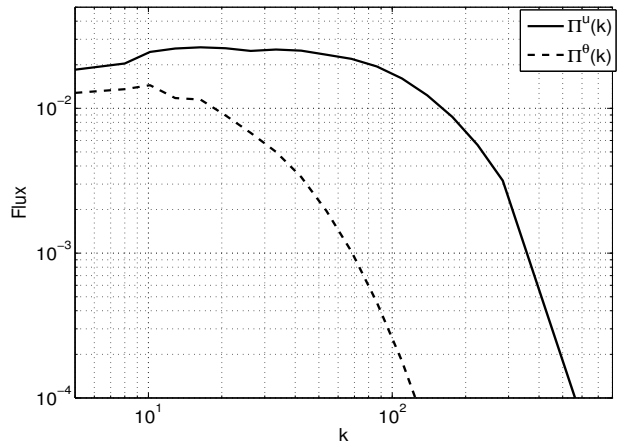

Figure 5. Kinetic energy flux (solid line) and the entropy flux (dashed line) for $R = 2.6 \times 10^6$ and $P = 0.02$ on a 512^3 grid. The constant behaviour of kinetic energy flux in the narrow inertial range indicate the general agreement with KO scaling. The entropy flux decays exponentially. This Figure is taken from Mishra & Verma (2010).

exhibits plots of the compensated kinetic energy spectra $E^u(k)k^{5/3}$ and $E^u(k)k^{11/5}$ vs. k. The spectra and flux results are not conclusive for this case, yet, the BO scaling appears to fits better than the KO scaling for the compensated kinetic energy in the narrow range of wavenumbers. As the Kolmogorov length scale is of the order of Bolgiano length scale, we observe only BO scaling in inertial range for our simulation (Mishra & Verma (2010)). The entropy spectrum, shown in Fig. 7, has dual branches in the spectrum, similar to the low-Prandtl number case presented above. The upper branch fits well with the k^{-2} line, however, the lower branch tends to fit better with $k^{-7/5}$ line indicating the BO scaling for entropy spectrum (Mishra & Verma (2010)).

The kinetic energy and the entropy fluxes for $P = 6.8$ are plotted in Fig. 8. We find that the kinetic flux ($\Pi^u(k)$) falls quite sharply, but the compensated kinetic flux ($\Pi^u(k)k^{4/5}$) exhibit a constant behaviour for a narrow range of wavenumbers. The constant nature of the entropy flux and the compensated kinetic flux support the BO scaling over the KO scaling for large-P convection.

We also simulated 2D RBC for $P = 1$ with no-slip boundary conditions at all the walls. For the temperature field, we applied constant temperature at the horizontal plates, and adiabatic boundary condition at the vertical plates. Numerical details are described briefly in Sec. 2. For the energy and entropy spectra, we interpolate the field variables to a uniform grid. In Fig. 9 we illustrate the kinetic energy spectrum, which appears to fit better with the BO scaling than the KO scaling. The entropy spectrum shown in Fig. 10 has too much scatter to be able to make any conclusion. We plan to perform RBC simulations under no-slip boundary conditions for both 2D and 3D with much higher resolutions. These results will be presented in future.

4. Summary and Conclusions

We construct phenomenological arguments for the spectra of zero-P and low-P turbulent RBC. For zero-P convection, the temperature spectrum is very steep since $u_3 = \nabla^2\theta$, and the buoyancy force is effective only at low wavenumber modes. Consequently, the energy spectrum follows Kolmogorov 5/3 power law. For small-P, the Kolmogorov's diffusive wavenumber k_c is smaller than Kolmogorov's dissipative wavenumber k_d. Consequently, for $k_c < k < k_d$, we expect 5/3

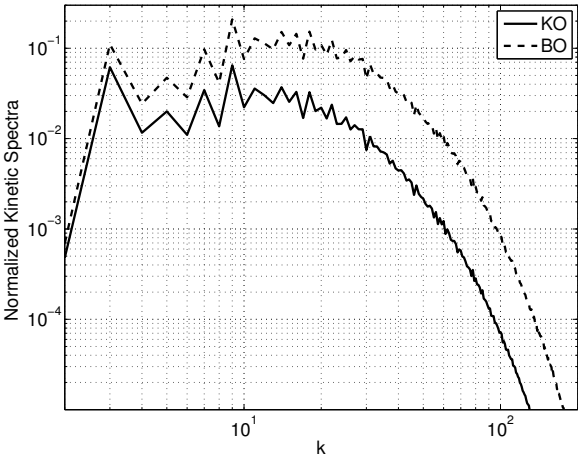

Figure 6. Compensated kinetic energy spectra $E^u(k)k^{5/3}$ (KO) and $E^u(k)k^{11/5}$ (BO) for $P = 6.8$ and $R = 6.6 \times 10^6$ on a 512^3 grid. The results are somewhat inconclusive, yet the BO scaling is in better agreement with the numerical data than the KO scaling. This Figure is taken from Mishra & Verma (2010).

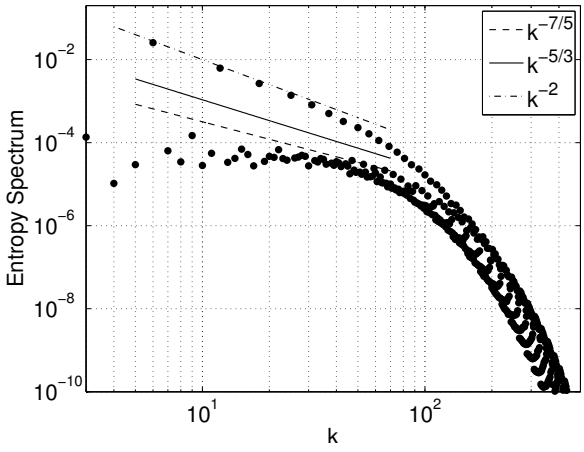

Figure 7. Entropy spectrum $E^\theta(k)$ for $P = 6.8$ and $R = 6.6 \times 10^6$ on a 512^3 grid. BO scaling tend to fit better compared to the KO scaling for lower part of the spectrum. The upper branch fits with k^{-2} quite well. This Figure is taken from Mishra & Verma (2010).

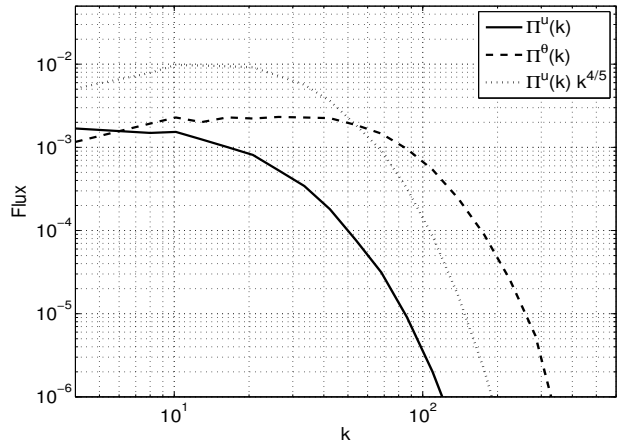

Figure 8. kinetic energy flux (solid line) and the entropy flux (dashed line) for $R = 6.6 \times 10^6$ and $P = 6.8$ on a 512^3 grid. $\Pi^\theta(k)$ and the normalized kinetic energy flux (multiplied by $k^{4/5}$), shown as a dotted line, are constant for a range of wavenumbers. This Figure is taken from Mishra & Verma (2010).

power law spectrum the velocity field, and an exponential spectrum for the temperature field.

We performed numerical simulations of turbulent RBC flows for zero-Prandtl number, low-Prandtl number ($P = 0.02$), and large-Prandtl number ($P = 6.8$) and computed the energy spectra and fluxes. The numerical results of zero-P and low-P RBC are in very good agreement with the above phenomenological arguments. However, for the temperature field, we obtain dual spectrum with one of them being k^{-2} corresponding to $\theta(0, 0, 2n)$ modes.

The spectra for the large-P case is quite ambiguous for the resolutions used in the simulations. However, the BO scaling appears to be closer to the numerical results than the KO scaling. We

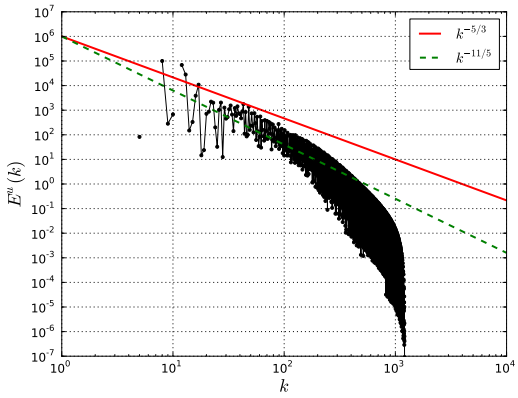

Figure 9. Kinetic energy spectrum $E^u(k)$ for $R = 2 \times 10^7$ and $P = 1$ obtained from a 2D RBC simulation with no-slip boundary conditions. The numerical results are in better agreement with the BO scaling than the KO scaling.

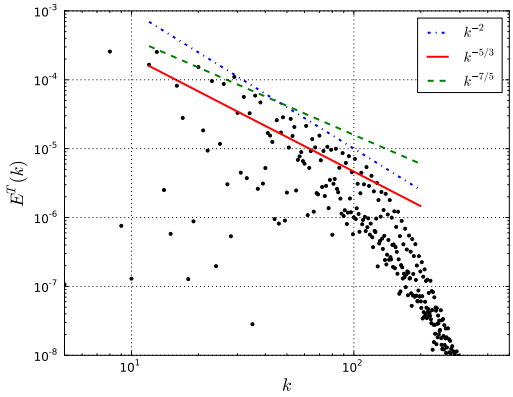

Figure 10. Entropy spectrum $E^\theta(k)$ for $R = 2 \times 10^7$ and $P = 1$ obtained from a 2D RBC simulation with no-slip boundary conditions. The numerical data has a large scatter.

need to perform higher resolution simulations to resolve this issue. Also, structure function and anisotropy studies would yield further insights into the nature of turbulence. We need to perform high resolution numerical simulations for the no-slip boundary conditions for a detailed study of the nature of turbulence in the bulk and in the boundary layers.

Acknowledgments

We thank Stephan Fauve and Sandeep Reddy for very useful discussions. We are grateful to Paul Fischer and other developers of NEK5000 for providing valuable assistance during our work on NEK5000. We also thank Computational Research Laboratory (CRL) and Centre for Development of Advanced Computing (CDAC) for providing us computing time on EKA and PARAM YUVA respectively. Part of this work was supported by Swarnajayanti fellowship to MKV, and BRNS grant BRNS/PHY/20090310.

References

Ashkenazi, S. & Steinberg, V. 1999 Spectra and statistics of velocity and temperature fluctuations in turbulent convection. *Phys. Rev. Lett.* **83**, 4760.

Borue, V. & Orszag, S. 1997 Turbulent convection driven by a constant temperature gradient. *Journal of Scientific Computing* **12**, 305–351.

Castaing, B. 1990 Scaling of turbulent spectra. *Phys. Rev. Lett.* **65**, 3209.

Chilla, F., Ciliberto, S., Innocenti, C. & Pampaloni, E. 1993 Boundary layer and scaling properties in turbulent thermal convection. *Il Nuovo Cimento D* **15**, 1229.

Cioni, S., Ciliberto, S. & Sommeria, J. 1995 Temperature structure functions in turbulent convection at low prandtl number. *Europhys Lett* **32**, 413–418.

Cioni, S., Ciliberto, S. & Sommeria, J. 1997 Strongly turbulent rayleigh–bénard convection in mercury: comparison with results at moderate prandtl number. *J. Fluid Mech.* **335**, 111.

Fischer, P. F. 1997 An overlapping schwarz method for spectral element solution of the incompressible navier–stokes equations. *J. Comp. Phys.* **133**, 84.

Grossmann, S. & Lohse, D. 1991 Fourier-weierstrass mode analysis for thermally driven turbulence. *Phys. Rev. Lett.* **67**, 445–448.

Grossmann, S. & Lohse, D. 1992 Scaling in hard turbulent rayleigh-benard flow. *Phys. Review A* **46**, 903–917.

Grossmann, S. & Lohse, D. 2000 Scaling in thermal convection: a unifying theory. *J. Fluid Mech.* **407**, 27.

Grossmann, S. & L'vov, V. 1993 Crossover of spectral scaling in thermal turbulence. *Phys. Rev. E* **47**, 4161–4168.

Kerr, R. 1996 Rayleigh number scaling in numerical convection. *J. Fluid Mech.* **310**, 139–179.

Kraichnan, R. H. 1962 Turbulent thermal convection at arbtrary prandtl number. *Phys. Fluids* **5**, 1374.

Lesieur, L. 2006 *Turbulence in Fluids*, 4th edn. Dordrecht: Springer.

Lohse, D. & Xia, K. Q. 2010 Small-scale properties of turbulent rayleigh-bénard convection. *Ann. Rev. Fluid Mech.* **42**, 335–364.

L'vov, V. 1991 Spectra of velocity and temperature fluctuations with constant entropy flux of fully developed free-convective turbulence. *Phys. Rev. Lett.* **67**, 687.

L'vov, V. & Falkovich, G. 1992 Conservation-laws and 2-flux spectra of hydrodynamic convective turbulence. *Physica D* **57**, 85–95.

Mashiko, T., Tsuji, Y., Mizuno, T. & Sano, M. 2004 Instantaneous measurement of velocity fields in developed thermal turbulence in mercury. *Phys. Rev. E* **69**, 036306.

Mishra, P. K. & Verma, M. K. 2010 Energy spectra and fluxes for rayleigh-bénard convection. *Phys. Rev. E* **81**, 056316.

Niemela, J. J., Skrbek, L., Sreenivasan, K. R. & Donnelly, R. J. 2000 Turbulent convection at very high rayleigh number. *Nature* **404**, 837–840.

Procaccia, I. & Zeitak, R. 1989 Scaling exponents in nonisotropic convective turbulence. *Phys. Rev. Lett.* **62**, 2128–2131.

Shang, X. & Xia, K. 2001 Scaling of the velocity power spectra in turbulent thermal convection. *Phys. Rev. E* **64**, 065301.

Siggia, E. D. 1994 High rayleigh number convection. *Ann. Rev. Fluid Mech.* **26**, 137.

Skandera, D., Busse, A. & W.-c, Müller. 2009 Scaling properties of convective turbulence. *High Performance Computing in Science and Engineering, Garching/Munich 2007, Springer Berlin Heidelberg* p. 387.

Sun, C., Zhou, Q. & Xia, K. 2006 Cascades of velocity and temperature fluctuations in buoyancy-driven thermal turbulence. *Phys. Rev. Lett.* **97**, 144504.

Verma, M. K. 2004 Statistical theory of magnetohydrodynamic turbulence: Recent results. *Phys. Rep.* **401**, 229–380.

Vincent, A. P. & Yuen, D. A. 1999 Plumes and waves in two-dimensional turbulent thermal convection. *Physical Review E (Statistical Physics* **60**, 2957.

Wu, X., Kadanoff, L., Libchaber, A. & Sano, M. 1990 Frequency power spectrum of temperature fluctuations in free convection. *Phys. Rev. Lett.* **64**, 2140–2143.

Zhou, S. & Xia, K. 2001 Scaling properties of the temperature field in convective turbulence. *Physical review letters* **87**, 064501.